Pressure evaluation of spray induced flow by means of URANS and time-resolved Stereo Particle Image Velocimetry

N. Kling[1,2,*], L. Opfer[1], J. Kriegseis[2], P. Rogler[1],
1: Powertrain Solutions, Robert Bosch GmbH, Germany
2: Institute of Fluid Mechanics, Karlsruher Institute of Technology, Germany
* Correspondent author: Nils.Kling@de.bosch.com

Keywords: Pressure evaluation, spray induced flow, URANS, SPIV, LIF, ensemble averaging

ABSTRACT

In the present work, pressure distributions of spray-induced flow are obtained by means of time-resolved stereo Particle Image Velocimetry. Revealing an extensive insight in the nature of spray transport, the characterization of pressure, material acceleration and instantaneous velocity provides a comprehensive description of spray induced flow dynamics. The pressure evaluation is conducted by an extended formulation based on the Unsteady Reynolds Averaged Navier-Stokes Equations and ensemble averaging. Assuming adiabatic flow and perfect gas the effect of compressibility is taken into account. In order to achieve phase discrimination and image contrast enhancement, optical filtering is applied by doping the gaseous phase with fluorescent tracer particles. The measurements are performed with gasoline direct injection 2-hole research samples. Demonstrating the capacity of pressure evaluation, pressure fields of spray-induced flow are successfully obtained. The investigations reveal characteristic flow patterns in accordance to air entrainment and fluid displacement. In respect to single spray plumes, high pressure regions are identified in front of the spray and the wake flow, whereas low pressure regions are present at central position. The pressure evaluation exposes minimal pressure differences.

1. Introduction

The development of modern gasoline direct injection engines is driven by a constant effort to minimize emissions and improve efficiency. A particular focus is the reduction of particulate emissions. In this context, processes of mixture preparation are highly relevant. The mechanisms of mixture preparation depend strongly on thermodynamic engine conditions such as inner flow, fuel temperature, fuel pressure, cylinder temperature and backpressure. Macroscopic spray features such as axial and radial penetration, spray angle and spray patterns show different behaviour for various conditions. Considering additional phenomena like flashboiling and spray contraction, injector design and spray layout pursues optimal mixture preparation and the prevention of fuel impingement on combustion chamber walls in order to achieve high quality combustion and low emission for the entire engine operating map.

Depending on the focus of interest, such as internal nozzle flow, near-field spray-formation, far-field developed spray, a wide range of measurement techniques are utilized for spray analysis. In

addition to classic experimental approaches for spray feature characterisation, measurement techniques are applied to cover quantities such as velocity, density, temperature, fluxes, geometries and distributions. A broad documentation and classification of available measurement techniques are summarised in Fansler et al. (2015) and Tropea (2011).

Due to exchanges of mass, momentum and energy, strong interactions between spray and gas are present. As a result, the spray transport is highly affected by the flow of the surrounding gaseous phase. Based on the tracking behaviour of droplets, spray is accelerated and approaches the dynamic of gas. A complete description of the fluid dynamic is available by information about time-resolved velocity. In order to measure velocity fields Particle Image Velocimetry has been established in the past (Adrian (2005), Raffel et al. (2007)).

Due to increasing technical progress in the field of cameras, lasers and measurement methods (Stereo-PIV, Tomo-PIV, STB) Particle Image Velocimetry is able to provide time-resolved multi-dimensional velocity fields. The application of the PIV technique to gasoline direct injection sprays is a specific challenge due to very small time and length scales. The temporal dimension of injection, spray formation and spray transport is in order of few milliseconds. To perform time-resolved measurements high-speed laser and camera-techniques are required. Using classic Mie-scattering, scattered light intensities from liquid fuel are highly dominant over light being scattered by tracers inside the gaseous phase, resulting in noisy PIV data. In order to achieve phase discrimination and contrast enhancement, optical filtering by doping the gaseous phase with fluorescent tracer particles is applied.

In the present work, the flow dynamics of the gaseous phase is investigated by means of time-resolved stereo-fluorescence-PIV. The objective of the work is the experimental analysis of pressure distributions of spray induced flows in order to characterise spray transport. According to the momentum equations of fluid dynamics, the pressure gradient is coupled to density, viscous effects, volume forces and material acceleration. In general, sufficient information about velocity allows the evaluation of pressure fields. Theory and techniques of pressure evaluation are reviewed in van Oudheusden (2013).

An extended approach for pressure evaluation is presented and discussed. In order to obtain 3-dimensional velocity information due to stereo-PIV, the pressure evaluation is based on the Unsteady Reynolds Averaged Navier-Stokes equations (URANS) and ensemble averaging. In multiple measurement planes, ensemble-averaged velocity fields are merged to a 3-dimensional velocity field. Reynolds tensions occurring in the URANS-equations are characterised by the variance of the velocity fields. In order to account for compressibility an approach, which grounds on adiabatic flow and perfect gas assumptions, is applied (see van Oudheusden (2007)). Possible

evaporation effects, which would lead to differences in density, are neglected. Viscous effects are assumed to be of minor impact considering the order of magnitude for many flow applications.

2. Theoretical Background

Pressure evaluation by means of Particle Image Velocimetry relies on the inverse solution of the Navier-Stokes-equations. The Navier-Stokes-equations comprises information about velocity, material acceleration, density and viscosity. In the present work, a statistic formulation based on the Unsteady Reynolds Averaged Navier-Stokes-equations is presented. Due to low Mach numbers in the region of interest, the impact of density fluctuations are assumed as negligible. The corresponding URANS-equations are given by

$$\rho\frac{\partial\bar{u}_i}{\partial t}+\rho\bar{u}_j\frac{\partial\bar{u}_i}{\partial x_j}=\rho\frac{D\bar{u}_i}{Dt}=-\frac{\partial\bar{p}}{\partial x_i}+\frac{\partial}{\partial x_j}\left[\mu\left(\frac{\partial\bar{u}_i}{\partial x_j}+\frac{\partial\bar{u}_j}{\partial x_i}-\frac{2}{3}\delta_{ij}\frac{\partial\bar{u}_m}{\partial x_m}\right)\right]-\frac{\partial}{\partial x_j}\left(\rho\overline{\acute{u}_i\acute{u}_j}\right)+\rho\bar{f}_i \qquad (1)$$

where $\bar{p}$ is the mean pressure, $\bar{u}_i$ are the mean velocity components, ρ is the density, μ is the viscosity, $\bar{f}_i$ are the volumetric force components and $\left(\rho\overline{\acute{u}_i\acute{u}_j}\right)$ are the Reynolds tensions. The approach poses an extension of the mean pressure evaluation based on the RANS-equations (see e.g. Gurka et al. (1999)). Additionally it incorporates temporal flow evolution by introduction of a complementary term describing the local time change of momentum. In order to obtain sufficient velocity information for pressure evaluation by means of stereo-PIV, 3-dimensional velocity fields are obtained by ensemble averaging. The ensemble average is defined as the mean value of a quantity and can be determined by processing information of multiple similar experiments. The ensemble average of an arbitrary quantity θ is

$$\bar{\theta}(\mathbf{x},t)=\frac{\sum_{n=1}^{N}\bar{\theta}_n(\mathbf{x},t)}{N} \qquad (2)$$

where N is the number of experiments. In case of spray induced flow measurements, the ensemble average describes the mean behavior of several injections. Due to its stochastic nature, provoked by instabilities, turbulence, cavitation and other physically complex phenomena, the experiments are naturally not perfectly repeatable. The ensemble average contains therefore additional contributions of injection stochastic. The impact of the injection stochastic and the reliability will be investigated in the future.

In the following discussion, friction and volumetric forces are neglected. Consequently, the mean pressure gradient is described by material acceleration, Reynolds tensions and density.

$$\frac{\partial \bar{p}}{\partial x_i} = -\rho \frac{D\bar{u}_i}{Dt} - \frac{\partial}{\partial x_j}\left(\rho \overline{\acute{u}_i \acute{u}_j}\right) = -\rho\left(\frac{\partial \bar{u}_i}{\partial t} + \bar{u}_j \frac{\partial \bar{u}_i}{\partial x_j}\right) - \left(\frac{\partial \rho}{\partial x_j}\overline{\acute{u}_i \acute{u}_j} + \rho \frac{\partial \overline{\acute{u}_i \acute{u}_j}}{\partial x_j}\right) \tag{3}$$

Material acceleration and Reynolds tensions

The computation of material acceleration can be conducted with either a Lagrangian or Eulerian perspective. The Lagrangian approach relies on the perspective of a fluid particle, whereas the Eularian approach references to a stationary perspective. The Lagrangian and Eularian formulations are as follows

$$\frac{D\bar{u}_i}{Dt} = \frac{\partial \bar{u}_i}{\partial t} + \bar{u}_j \frac{\partial \bar{u}_i}{\partial x_j} = \frac{D\bar{u}_i(\varepsilon(\mathbf{x}_0, t_0), t)}{Dt} \tag{4}$$

where ε is the trajectory of a particle and its related position x_0 at time t_0. In the present work, the computation of material acceleration relies on an Eularian perspective. The Reynolds tensions are described as the averaged product of corresponding velocity fluctuations.

$$\overline{\acute{u}_i \acute{u}_j} = \frac{1}{N}\sum_{n=1}^{N} \acute{u}_{i,n} \acute{u}_{j,n} \tag{5}$$

Pressure gradient integration

The pressure computation is based on the spatial integration of the pressure gradient. The partial differential equation requires the definition and implementation of boundary conditions. In the past, two different integration-strategies have been employed. One of the strategies is a spatial marching scheme (see e.g. Baur et al. (1999)), whose procedure describes the direct integration of the pressure gradient along a specified marching route in the domain of interest. The other strategy is the formulation of a Poisson equation and its subsequent solving. In the present work, the pressure computation is performed by utilizing the Poisson equation. The Poisson equation is retrieved by the divergence of the pressure gradient.

$$\begin{aligned}\frac{\partial^2 \bar{p}}{\partial x_i \, \partial x_i} = &-\frac{\partial \rho}{\partial x_i}\left(\frac{\partial \bar{u}_i}{\partial t} + \bar{u}_j \frac{\partial \bar{u}_i}{\partial x_j}\right) - \rho\left(\frac{\partial^2 \bar{u}_i}{\partial t \, \partial x_i} + \frac{\partial \bar{u}_j}{\partial x_i}\frac{\partial \bar{u}_i}{\partial x_j} + \bar{u}_j \frac{\partial^2 \bar{u}_i}{\partial x_i \, \partial x_j}\right) \\ &+ \left(\frac{\partial^2 \rho}{\partial x_j \, \partial x_i}\overline{\acute{u}_i \acute{u}_j} + \frac{\partial \rho}{\partial x_j}\frac{\partial \overline{\acute{u}_i \acute{u}_j}}{\partial x_i} + \rho \frac{\partial^2 \overline{\acute{u}_i \acute{u}_j}}{\partial x_j \, \partial x_i}\right)\end{aligned} \tag{6}$$

In case of negligible density gradients and divergence-free flow, equation (6) can be further simplified. Considering divergence-free flow, the Poisson equation becomes time-independent. Furthermore, most of the terms on the right hand side disappear by vanishing density gradients.

Compressibility

In order to consider compressible flow, a description of the density dependency has to be introduced. Souverein et al. (2007) proposed an eligible formulation, which grounds on adiabatic flow assumption and perfect gas law. The perfect gas law allows the substitution of density in terms of pressure and temperature. In consequence of the adiabatic flow assumption, the temperature relates directly to the velocity information. The mean temperature yields

$$\frac{\overline{\mathrm{T}}}{\overline{\mathrm{T}}_\infty} = 1 + \frac{\gamma - 1}{2}\overline{\mathrm{M}}_\infty^2 \left(1 - \frac{\overline{\mathrm{V}}^2}{\overline{\mathrm{V}}_\infty^2}\right) \tag{7}$$

where $\overline{\mathrm{T}}_\infty$, $\overline{\mathrm{M}}_\infty$, $\overline{\mathrm{V}}_\infty$ are the mean environmental quantities for temperature, Mach number and absolute velocity; γ is the heat capacity ratio.

Introducing the perfect gas law, the formulations of the URANS-equation (5) and the Poisson equation (6) are described as follows

$$\left(\delta_{ij} + \frac{\overline{\acute{\mathrm{u}}_\mathrm{i}\acute{\mathrm{u}}_\mathrm{j}}}{R\overline{T}}\right)\frac{\partial \ln\left(\frac{\overline{\mathrm{p}}}{\bar{p}_\infty}\right)}{\partial \mathrm{x_j}} = -\frac{1}{\mathrm{R}\overline{\mathrm{T}}}\left(\frac{\partial \bar{\mathrm{u}}_\mathrm{i}}{\partial \mathrm{t}} + \bar{\mathrm{u}}_\mathrm{j}\frac{\partial \bar{\mathrm{u}}_\mathrm{i}}{\partial \mathrm{x_j}} + \frac{\partial \overline{\acute{\mathrm{u}}_\mathrm{i}\acute{\mathrm{u}}_\mathrm{j}}}{\partial \mathrm{x_j}} - \frac{\overline{\acute{\mathrm{u}}_\mathrm{i}\acute{\mathrm{u}}_\mathrm{j}}}{\overline{\mathrm{T}}}\frac{\partial \overline{\mathrm{T}}}{\partial \mathrm{x_j}}\right) \tag{8}$$

$$\begin{aligned}\frac{\partial^2 \ln\left(\frac{\overline{\mathrm{p}}}{\bar{p}_\infty}\right)}{\partial \mathrm{x_i}\,\partial \mathrm{x_i}} + \frac{1}{R\overline{\mathrm{T}}}\overline{\acute{\mathrm{u}}_\mathrm{i}\acute{\mathrm{u}}_\mathrm{j}}\frac{\partial^2 \ln\left(\frac{\overline{\mathrm{p}}}{\bar{p}_\infty}\right)}{\partial \mathrm{x_i}\,\partial \mathrm{x_j}} + \frac{1}{R\overline{\mathrm{T}}}\frac{\partial \ln\left(\frac{\overline{\mathrm{p}}}{\bar{p}_\infty}\right)}{\partial \mathrm{x_i}}\left(\frac{\partial \bar{\mathrm{u}}_\mathrm{i}}{\partial \mathrm{t}} + \bar{\mathrm{u}}_\mathrm{j}\frac{\partial \bar{\mathrm{u}}_\mathrm{i}}{\partial \mathrm{x_j}} + \frac{\partial \overline{\acute{\mathrm{u}}_\mathrm{i}\acute{\mathrm{u}}_\mathrm{j}}}{\partial \mathrm{x}_j}\right) \\ = -\frac{1}{R\overline{\mathrm{T}}^2}\frac{\partial \overline{\mathrm{T}}}{\partial \mathrm{x_i}}\left(\frac{\partial \bar{\mathrm{u}}_\mathrm{i}}{\partial \mathrm{t}} + \bar{\mathrm{u}}_\mathrm{j}\frac{\partial \bar{\mathrm{u}}_\mathrm{i}}{\partial \mathrm{x_j}} + \frac{\partial \overline{\acute{\mathrm{u}}_\mathrm{i}\acute{\mathrm{u}}_\mathrm{j}}}{\partial \mathrm{x}_j}\right) - \frac{1}{R\overline{\mathrm{T}}}\left(\frac{\partial^2 \bar{\mathrm{u}}_\mathrm{i}}{\partial \mathrm{t}\,\partial \mathrm{x_i}} + \frac{\partial \bar{\mathrm{u}}_\mathrm{i}}{\partial \mathrm{x_j}}\frac{\partial \bar{\mathrm{u}}_\mathrm{j}}{\partial \mathrm{x_i}} + \bar{\mathrm{u}}_\mathrm{j}\frac{\partial^2 \bar{\mathrm{u}}_\mathrm{i}}{\partial \mathrm{x_i}\,\partial \mathrm{x_j}}\right) \\ - \frac{1}{R\overline{\mathrm{T}}}\left[\left(-\frac{2}{\overline{\mathrm{T}}^2}\frac{\partial \overline{\mathrm{T}}}{\partial \mathrm{x_i}}\frac{\partial \overline{\mathrm{T}}}{\partial \mathrm{x_j}} + \frac{1}{\overline{\mathrm{T}}}\frac{\partial^2 \overline{\mathrm{T}}}{\partial \mathrm{x_j}\,\partial \mathrm{x_i}}\right)\overline{\acute{\mathrm{u}}_\mathrm{i}\acute{\mathrm{u}}_\mathrm{j}} + \frac{\partial^2 \overline{\acute{\mathrm{u}}_\mathrm{i}\acute{\mathrm{u}}_\mathrm{j}}}{\partial \mathrm{x_j}\,\partial \mathrm{x_i}}\right]\end{aligned} \tag{9}$$

where R is the specific gas constant. Due to the application of the perfect gas law, the primary Poisson equation becomes a second order partial differential equation with mixed partial derivatives. For the solution of the partial differential equation, the implementation of proper boundary condition has to be conducted. In principal, two different types of boundary conditions are employed. Firstly, the description of boundary conditions via Dirichlet boundary conditions,

which determine pressure values directly, and secondly Neumann boundary conditions, which describe the pressure gradient characterized by the momentum equation (8). In the present work, the boundary conditions are mainly set to Neumann boundary conditions. A single Dirichlet boundary condition is implemented at a position with minimal temporal mean pressure gradient, describing the pressure field unambiguously.

2. Experimental Assembly

A cubic pressure chamber with optical access due to glass windows frames the injection and the corresponding two-phase flow. To ensure inertisation, the pressure chamber operates with a nitrogen atmosphere. The nitrogen volume flux through the chamber is limited to an amount that does not affect the spray-induced gas flow. The measurement setup is illustrated in figure 1. The injector placement is at top center position.

In reference to figure 2, the stereo-PIV setup is in front of the pressure chamber, whereas the laser-light-sheet is introduced from right hand side. The relative angle between the cameras and the perpendicular is approx. 16 degrees. The measurement equipment consisting of two high-speed CMOS cameras (Phantom V1612) and a double-pulsed Nd-YAG laser (DM100-532) allows for time-resolved measurements. The cameras are equipped with AF-S NIKKOR 105 mm lenses. The optical setup yields a spatial resolution of approx. 10 pixels/mm. The frequency-doubled laser operates with a wavelength of 532 nm, enabling time-resolved measurement of spray induced flow. An average power of 100 W and a pulse energy of 10 mJ are available at a frequency of 10 kHz. In order to achieve phase discrimination and contrast enhancement, fluorescent tracer particles are employed. Referring to the study of Rottenkolber et al. (2003), the applied tracer particles are a solution of fluorescent dye (DCM) and Propylene Carbonate. The beneficial properties of the solution are a high fluorescent emission and a strong frequency shift. Applying optical filtering, the frequency shift allows a very good suppression of the initial wavelength scattered by the spray. The optical filtering is realised with OD 4 short-pass filters with a cut-off wavelength of 600 nm. The setup yields a high quality of raw images, beeing a reliable basis for PIV postprocessing and velocity computation.

The investigated gasoline direct injection nozzle is a two-hole research sample with spray hole inclination angles of 50 and 10 degrees. The orientation of the main injector axis is parallel to the laser light sheet. The rotation of the injector is adjusted so that both spray plumes are within the measurement plane. The gaseous phase is at a backpressure of 1 bar and a temperature of 25 °C, whereas the fuel injection pressure is set to 200 bar and the fuel temperature is 25 °C. The experiments are performed using n-Heptane as fuel.

The computation of the velocity is carried out with a multi-pass cross-correlation algorithm. Starting with an initial interrogation area size of 64x64 pixels, a final size of 24x24 is attained. Checking for data validity spurious vectors are identified and removed through a normalized median filter (3x3 neighborhood) (Westerweel (2005)).

In order to receive 3-dimensional ensemble averaged velocity fields, multiple experiments are executed in five parallel, equally spaced measurement planes. The distances between separate measurements planes are 1 mm, which ranges in the order of the interrogation area size. The procedure of ensemble averaging comprises of a contribution of 50 injection events per measurement plane. The acquisition frequency is 10 kHz with an inter-frame time of 10 µs. The pressure evaluation is conducted via an in-house Code. The measurement conditions and Stereo-PIV configurations are summarised in Table 1 and 2.

Table 1 Measurement conditions

Gaseous phase	
Species	N_2
Backpressure	1 bar
Temperature	25 °C
Liquid Fuel	
Species	n-Heptane
Pressure	200 bar
Temperature	25 °C

Table 2 Stereo-PIV configuration

Interrogation area size	24x24 pixels
Vector spacing	$\Delta x = \Delta y = 2{,}4$ mm; $\Delta z = 1$ mm
Acquisition frequency	10 kHz
Inter-frame time	10 µs
Measurement planes	5
Measurements per plane	50

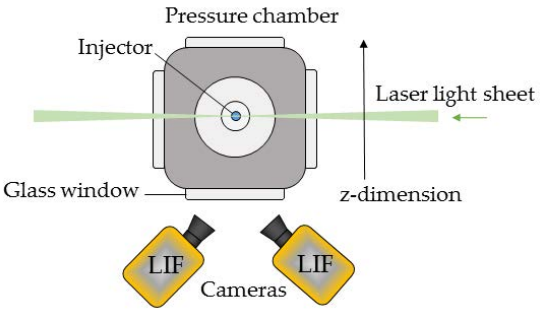

Fig. 1 Schematic illustration of the experimental assembly; Stereo-PIV configuration

3. Results

The velocity fields of spray-induced flow at two distinct timings are shown in figure 2. As a result of spray-air interaction due to exchange of momentum, the velocity fields indicate typical flow compositions displaying air entrainment and fluid displacement. Comparatively high velocities

concentrate in the immediate proximity of spray. Revealing an insight into the flow dynamics of spray induced flow, the corresponding material accelerations and pressure distributions are shown in figure 3. Referring to a single spray plume, high pressure regions are obtained at the spray plume tip and wake flow, whereas low pressures are present in the middle section. The pressure gradient in front of the spray plume tip accelerates fluid masses radially towards outward direction. Revealing the quality of air entrainment, the underlying fluid dynamic traces back to the low pressure region in the middle section. The dashed line between both spray plumes marks the separation of attraction. According to the position, whether on the right hand or left hand side, fluid masses are accelerated towards to the corresponding spray plume. At the saddle

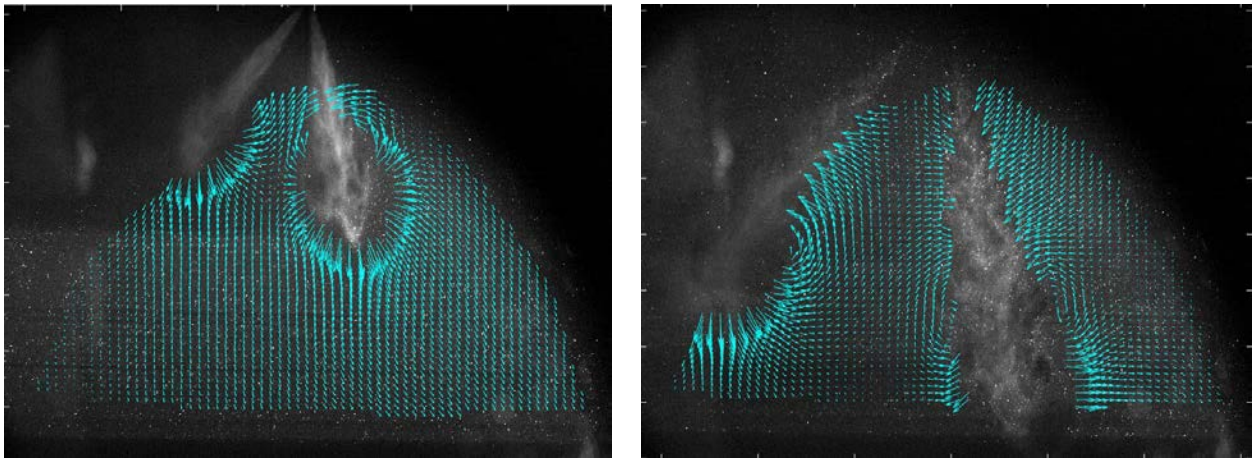

Fig. 2 Central measurement plane; ensemble averaged velocity field (cyan); background: raw image; left – early injection timing, right – late injection timing

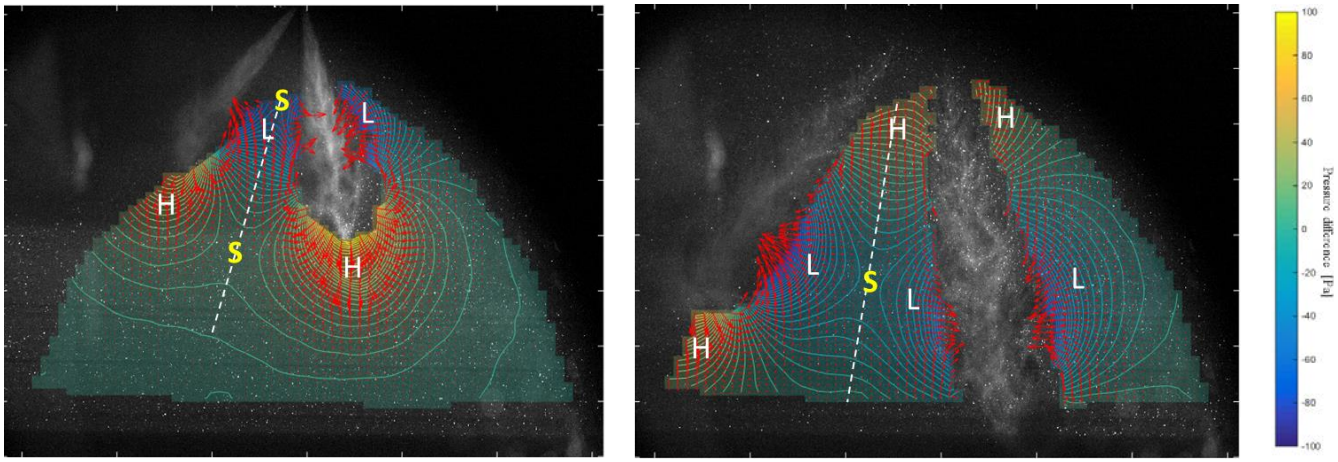

Fig. 3 Central measurement plane; Contour plot of pressure distribution relative to 1 bar absolute pressure; material acceleration vector field (red); background: raw image; left – early injection timing, right – late injection timing; (H) high pressure region, (L) low pressure region; dashed line – vanishing material acceleration towards singular spray plumes; Saddle point (S) – no material acceleration

points the pressure gradients vanish leading to no instantaneous accelerations. Depending on the orientation, saddle points act either stable or unstable as well as attracting or repulsing. The foremost saddle point is unstable and repulsive in the direction of the dashed line, whereas stable and attracting perpendicular to it. The resulting pressure differences are in the order of magnitude of 0.1 mbar.

4. Conclusion

Time-resolved pressure fields are obtained for spray-induced flow, demonstrating the capacity of pressure evaluation by means of Particle Image Velocimetry. In order to obtain 3-dimensional velocity information in the framework of stereo-PIV, an extended formulation based on the URANS-equations is successfully applied. Missing flow information are compensated due to ensemble averaging and the consequential construction of 3-dimensional velocity fields. Compressibility effects are incorporated assuming adiabatic flow and prefect gas conditions, density fluctuations and viscous effects are neglected. The computation of material acceleration relies on an Eularian perspective. The pressure gradient integration strategy is based on the divergence of URANS-equations. Implementing the perfect gas law, the original Poisson-equation is extended by additional first and second order partial derivatives. The utilized boundary conditions are mainly Neumann except for a single Dirichlet boundary condition in order to describe the solution of the partial differential equation unambiguously.
The pressure distributions of spray-induced flow reveal characteristic flow patterns in the vicinity of spray. High-pressure regions are observed in front of spray plume tips and wake flow, whereas low pressure regions are present in the middle section. The high pressure regions at the spray plume tips cause radial displacements in front of the spray. Disclosing the flow dynamics of air entrainment, attracting low pressure regions accelerate fluid masses towards the spray. The pressure distributions indicate low pressure differences in the order of 0.1 mbar.
Demonstrating the capacity of pressure evaluation by means of Particle Image Velocimetry, a comprehensive characterization of the fluid dynamics of spray-induced flow and thereby spray is obtained.

5. References

Adrian RJ (1991) Particle-imaging techniques for experimental fluid mechanics. Annual Review of Fluid Mechanics 23(1):261–304

Baur T, Köngeter J (1999) PIV with high temporal resolution forthe determination of local pressure reductions from coherent turbulent phenomena. 3rd Int. Workshop on Particle Image Velocimetry (Santa Barbara) pp 101–6

Fansler TD, Parrish SE (2015) Spray measurement technology: a review. Meas Sci Technol 26:012002

Gurka R, Liberzon A, Hefetz D, Rubinstein D, Shavit U (1999) Computation of pressure distribution using PIV velocity data. 3rd Int. Workshop on Particle Image Velocimetry (Santa Barbara) pp 671–6

Raffel M, Willert CE, Kompenhans J et al (2013) Particle image velocimetry: a practical guide. Springer

Rottenkolber G, Gindele J, Raposo J, Dullenkopf K, Hentschel W, Wittig S, Spicher U, Merzkirch W (2003) Spray analysis of a gasoline direct injector by means of two-phase PIV. Exp Fluids 32:710–721

Souverein L J, Van Oudheusden BW, Scarano F (2007) Particle image velocimetry based loads determination in supersonic flows 45th AIAA Aerosp. Science Meeting & Exhibit (Reno, NV) Paper AIAA-2007-0050

Tropea C (2011) Optical Particle Characterization in Flows. Annual Review of Fluid Mechanics Vol. 43:399-426

Van Oudheusden BW (2008) Principles and application of velocimetry-based planar pressure imaging in compressible flows with shocks. Exp Fluids 45:657–674

Van Oudheusden BW (2013) PIV-based pressure measurement. Meas Sci Technol 24(3):032001

Westerweel J, Scarano F (2005) Universal outlier detection for PIV data. Exp Fluids 39: 1096–1100